Journal of Alloys and Compounds 509 (2011) 3837–3842

Contents lists available at ScienceDirect

Journal of Alloys and Compounds

journal homepage: www.elsevier.com/locate/jallcom

Piezoelectric properties of Li–Ta co-doped potassium–sodium niobate ceramics prepared by spark plasma and conventional sintering

Rigoberto López-Juárez [a,*], Federico González-García [b], Juan Zárate-Medina [c], Ricardo Escalona-González [d], Sebastián Díaz de la Torre [d], María-Elena Villafuerte-Castrejón [a]

[a] Instituto de Investigaciones en Materiales, Universidad Nacional Autónoma de México, A.P. 70-360, México, D.F., Mexico
[b] Departamento de Ingeniería de Procesos e Hidráulica, Universidad Autónoma Metropolitana-Iztapalapa, A.P. 55-534, C.P. 09340, México, D.F., Mexico
[c] Instituto de Investigaciones Metalúrgicas, UMSNH, C.P. 58000, Morelia, Michoacán, Mexico
[d] Instituto Politécnico Nacional, Centro de Investigación e Innovación Tecnológica CIITEC, C.P. 02250, Azcapotzalco, México, D.F., Mexico

ARTICLE INFO

Article history:
Received 29 June 2010
Received in revised form
15 December 2010
Accepted 15 December 2010
Available online 22 December 2010

Keywords:
Ceramics
Sintering
Dielectric response
Piezoelectricity

ABSTRACT

Lead-free piezoelectric ceramics with $(K_{0.48}Na_{0.52})_{0.96}Li_{0.04}Nb_{0.85}Ta_{0.15}O_3$ composition were sintered by conventional pressureless (PLS) and spark plasma sintering (SPS) techniques. A comparative analysis of the sintering effect on the piezoelectric and dielectric properties was conducted. The SPS treated specimen revealed an enhancement in the piezoelectric properties as compared to the PLS counterpart. The piezoelectric and dielectric parameters of PLS sintered sample were $k'_p = 0.41$, $s'^{E}_{11} = 11.80 \times 10^{-12}$ m^2/N, $d'_{31} = -55.7$ (pC/N), $\varepsilon'^{T}_{33} = 464.5$ and $\tan\delta = 0.010$ at 10 kHz, whereas these parameters for the SPS sintered sample were $k'_p = 0.50$, $s'^{E}_{11} = 12.20 \times 10^{-12}$ m^2/N, $d'_{31} = -66.17$ (pC/N), $\varepsilon'^{T}_{33} = 557.4$ and $\tan\delta = 0.024$ at 10 kHz. The piezoelectric properties enhancement of the SPS treated sample is attributed to, both the lower sintering temperature and the higher density achieved over the PLS sintered sample.

1. Introduction

Piezoelectric materials of the lead zirconate–titanate (PZT) family have found a wide number of applications due to the advantages derived from their electrical properties. Since the publication of Saito et al. [1], great progress has been made in research on lead-free compounds, such as bismuth–sodium titanates and potassium–sodium niobates, with or without additions of dopants that form solid solutions. A significant part of the research conducted on this subject seeks high-density products in order to enhance their electric and piezoelectric properties.

The basic problem found when working with alkaline niobates is the densification level achieved at high temperatures. That situation occurs since the alkaline elements undergo sublimation, which considerably changes the initial stoichiometry. This problem has been addressed through different methods, one of these involves densification improvement by the addition of some oxides, namely CuO, ZnO, MnO_2, CeO_2 [2–5]. According to these investigations, it is believed that these compounds form a liquid phase at low temperatures, thus promoting densification. Another approach involves addition of A and B elements into the ABO_3 structure of the $K_{0.5}Na_{0.5}NbO_3$ (KNN) solid solution. In the A-site, several cations can be added, i.e. Li^+, Ba^{2+}, La^{3+}, Bi^{3+}, whereas for the B-site it is possible to introduce Ti^{4+}, Sb^{5+} or Ta^{5+} [4,6–9]. The ion substitution can induce phase transformation and consequently a better performance of materials. A third way to improve densification is by reducing the particle size of the synthesized powders; however, since the conventional ceramic method does not achieve considerable reduction of particle size, only a few results have been reported using sol–gel and mechanochemical methods [10,11]. Furthermore, the chemical homogeneity of the KNN compound with Li^+ and Ta^{5+} dopants synthesized by the conventional solid-state reaction route has revealed an inhomogeneous distribution of Nb^{5+}, Ta^{5+}, K^+ and Na^+ cations, which leads to a considerable detriment of the piezoelectric properties, being one reason for the discrepancy among the data reported by several authors for the same or similar composition [12]. These and other discrepancies on the piezoelectric properties of these materials, reported by different authors can be summarized in the following statements: (1) the inhomogeneous distribution of cations occurs since ball milling does not provide sufficient energy for reducing particle size, which consequently enlarges the diffusion distances for cations, (2) the thermal treatment for several hours, at temperatures higher than 800 °C during the synthesis stage, could produce considerable losses of alkaline elements, generating samples with very different compositions,

* Corresponding author. Tel.: +52 55 56 22 46 41x24646; fax: +52 55 56 16 13 71.
E-mail address: rigobertolj@yahoo.com.mx (R. López-Juárez).

0925-8388/$ – see front matter © 2010 Elsevier B.V. All rights reserved.
doi:10.1016/j.jallcom.2010.12.103

and (3) since the ball milling process partially reduces particle size, the sintering step is not very effective. Thus, the aim of this work is to study the sintering process of lithium–tantalum co-doped KNN ceramics, as well as the sintering effect on their piezoelectric properties.

2. Experimental procedures

Lead-free piezoceramics with $(K_{0.48}Na_{0.52})_{0.96}Li_{0.04}Nb_{0.85}Ta_{0.15}O_3$ (KNLNT) composition were synthesized using the following precursors: Nb_2O_5 (99.99%), Ta_2O_5 (99.99%), K_2CO_3 (99.8%), Na_2CO_3 (99.9%), Li_2CO_3 (99.997%), HF (40 vol.%), NH_4OH (30 vol.%) and $C_6H_8O_7{\cdot}H_2O$ (99.9%). Initially, niobium and tantalum oxides were dissolved with hydrofluoric acid at 70 °C for 8 h. Then, ammonium hydroxide was added until complete precipitation of niobium and tantalum hydrated oxides, was observed. This precipitate was filtered and washed three times with de-ionized water. Subsequently, it was dissolved in a 0.35 M citric acid solution to form the corresponding citrate complex of niobium and tantalum, which is more stable and can be handled with no special atmosphere. The alkaline metals solution was prepared dissolving potassium, sodium and lithium carbonates into citric acid solution. The two solutions containing cations and citric acid were mixed and fed into a spray dryer (Yamato Mini Spray-Dryer ADL-31). The powder precursor was calcined from 600 to 900 °C to induce its crystallization [13].

In order to densify the powder, two sintering techniques were used. The first one is the common pressureless sintering (PLS), while the other is the spark plasma sintering (SPS) technique. With the PLS method, the previously calcined powder at 800 °C for 1 h was uniaxially pressed to form a disk shaped pellet before being sintered in a conventional furnace at 1120 °C for 2 h in air (hereafter called KNLNT-SD PLS). With the aim of examining changes in piezoelectric properties as a function of density, another powder-sample (named KNLNT-SD SPS) was densified with a commercial spark plasma sintering device (Sumitomo DR. Sinter 1050). In the second case, the powder was pre-loaded into a graphite-die set, axially pressed (70 MPa) and thermally treated up to 900 °C, setting a heating rate of 100 °C/min and a holding time no longer than 15 min, details of this technology can be found elsewhere [14,15]. This sample was further annealed for 2 h at 900 °C to eliminate oxygen vacancies. The density of the sintered samples was measured through the Archimedes method in distilled water. Powders and sintered samples were structurally characterized by X-ray diffraction analysis at room temperature using Cu Kα radiation in a Bruker Advanced D-8 diffractometer and morphologically analyzed by scanning electron microscopy (SEM) with a Leica Cambridge Stereoscan 440 microscope at 20 kV.

In order to measure the dielectric and piezoelectric properties, the sintered circular specimens were thoroughly polished, and then a conductive silver paste was deposited on both of their circular faces and annealed at 600 °C for 30 min. Dielectric and piezoelectric characterization was conducted by impedance and admittance measurements, respectively. The data were acquired by using an impedance analyzer (Agilent 4294A); the measurements were carried out over the frequency range of 10^2 to 10^7 Hz. The experiments were taken from 4 to 6 °C steps in proximity to the transition temperature; otherwise, the steps were monitored at 10 °C. The rms applied voltage was 0.5 V. Samples were left at the preset temperature until thermal equilibrium was reached. The experiments were performed from room temperature up to 600 °C in open atmosphere. Concerning the piezoelectric characterization, sintered specimens were placed into a silicone oil bath and poled under a dc electric field of 50 kV/cm at 130 °C for 30 min, and cooled down at room temperature while keeping the applied field. The poled samples were aged for 24 h before measuring the modulus of the admittance and its angle phase. Frequency sweeps were carried out around the fundamental and first overtone resonance and anti-resonance modes. The dielectric permittivity (ε^T_{33}), the compliances (s^E_{11} and s^E_{12}), and the piezoelectric coefficient (d_{31}), as well as the planar coupling factor (k_p) of a disk shaped piezoelectric ceramic were calculated according to the method proposed by Alemany et al. [16,17], which makes it possible to obtain these parameters in complex form, and to calculate their related losses.

3. Results and discussion

A scanning electron microscopy image of KNLNT powder calcined during 1 h at 800 °C is shown in Fig. 1. It can be seen that the synthesized powder consists of agglomerates with primary particles of approximately 100 nm. It is worth noting that this size cannot be obtained by the conventional ceramic method. It is known that spray drying eliminates solvents in a very short time promoting chemical homogeneity on the precursor powders [18,19]. Additionally, powder calcination induces chemical reactions, which can produce gas formation as well as fine particles agglomeration. The small particle size observed is attributed to the presence of tantalum, which might act as a grain growth inhibitor, as it has been reported elsewhere to occur when added to KNN [20,21].

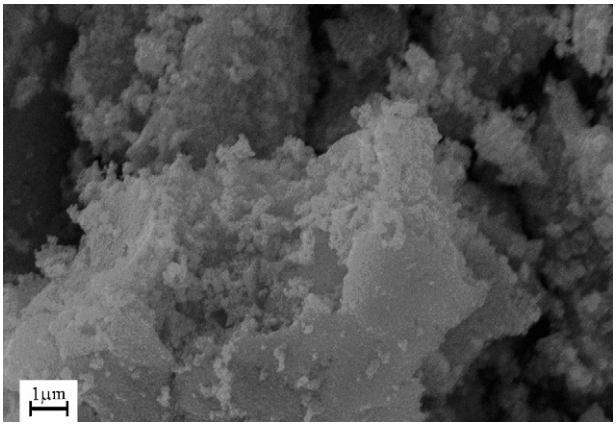

Fig. 1. SEM image of KNLNT powder calcined at 800 °C for 1 h.

The X-ray diffraction patterns obtained from the as-prepared precursor and those from the thermally annealed powders between 600 and 900 °C are shown in Fig. 2. It can be observed that the as-prepared dried powders are completely amorphous; this could be attributed to the rapid solvent elimination and the interaction of the different ions in solution with the citric acid. When the powder was thermally treated at 600 °C, several new diffraction traces appeared as small peaks, corresponding to the $K_3Li_2Nb_5O_{15}$ tetragonal secondary phase (JCPDS-ICDD 52-0157). These Bragg-planes coexist with the main reflections of the KNLNT phase. From Fig. 2, it is also evident that the presence of the secondary phase diminishes considerably for the sample calcined at 750 °C and at 800 °C, only the reflections corresponding to the KNLNT phase can be observed. These results are in good agreement with the fact that the synthesis of the KNN and related compositions through the conventional ceramic method [5,12,20–23] require ball-mill processing of powder from 4 to 24 h and its calcination from 750 to 850 °C over a long period of time. Higher temperatures cannot, in principle, guarantee stoichiometry and homogeneous distribution of the ions involved, as well as small particle size due to considerable sublimation of alkali cations and grain growth. Therefore, the spray drying step, as reported here, is important to crystallize powders, i.e. by setting a calcination time of 1 h at 800 °C. The reduction of calcination time leads to powder formation, which undergoes a small deviation from the initial stoichiometry and the small particle size of the powders promotes sinterability.

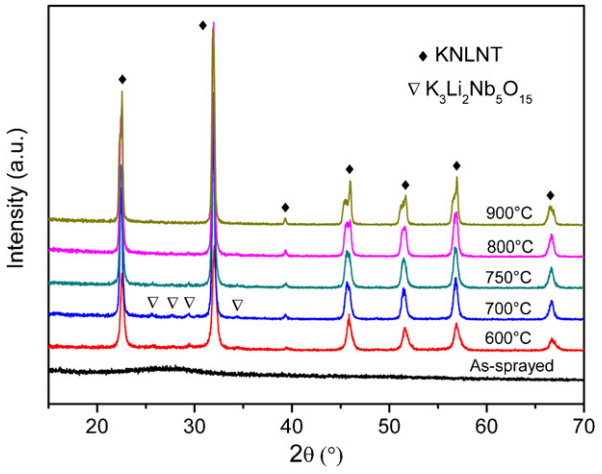

Fig. 2. X-ray diffraction pattern of KNLNT precursor powder and those obtained as a function of heating temperature.

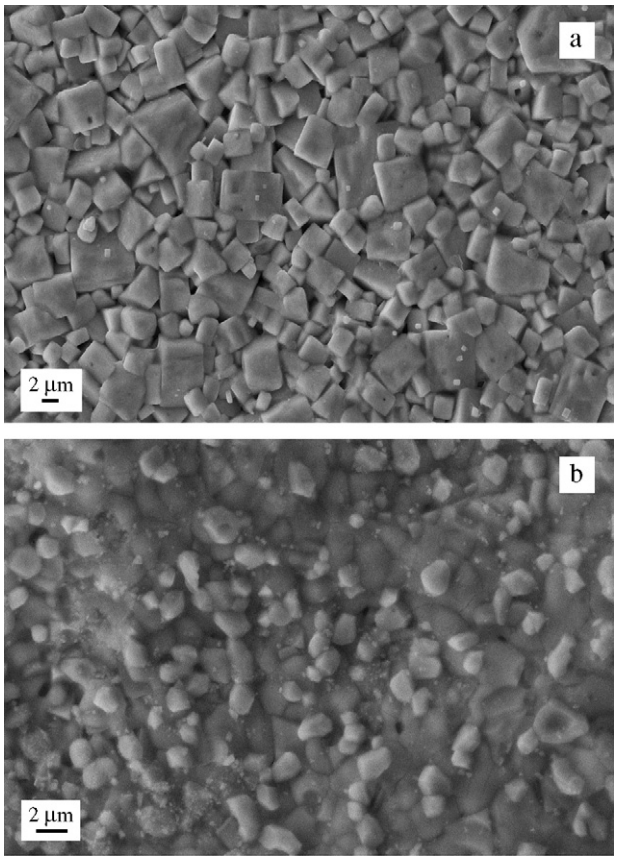

Fig. 3. SEM surface images of (a) KNLNT-SD PLS 1120 °C and (b) KNLNT-SD SPS 900 °C.

Scanning electron microscopy images of specimens conventionally sintered by PLS at 1120 °C and SPS-treated at 900 °C are shown in Fig. 3, respectively. It can be seen from Fig. 3(a) that the grains have developed a pseudo-cubic shape, which is a common feature of KNN compounds. This feature is typical in KNN compounds since they crystallize under orthorhombic or tetragonal structures at room temperature, depending either on the amount or type of dopants added to form a polymorphic phase boundary (PPB). It is well known that internal structure dictates the crystal morphology of materials [24,25]; this is related to the type of faces, and the energy required for the attachment of a new layer. These faces are commonly of low index (i.e. 1 0 0, 0 1 0, 1 1 1). Therefore, materials with tetragonal, orthorhombic or cubic structures grow under cuboid morphology where {1 0 0} faces are present.

According to the literature, Li^+ replaces K^+ and/or Na^+ in the A-site, whereas Ta^{5+} enters to the B-site in the perovskite structure. From Fig. 3(a) grains of 2 and 5 μm can also be observed. This behaviour in grain growth is attributed to the presence of tantalum, as it inhibits growth and leads to samples with homogeneous size distribution. The SPS-treated specimen (Fig. 3(b)) achieved considerably smaller particles as the result of a shorter holding time. By contrast to its counterpart, this specimen was sintered 220 °C lower than the PLS sintered specimen. The short sintering time set in SPS diminished alkaline element losses and inhibited grain growth. It is also evident that highest densification level was achieved in the SPS-treated sample. Such a difference on densification level has an important effect on their piezoelectric performance, as it will be shown next.

The X-ray diffraction patterns of the PLS-sintered sample at 1120 °C for 2 h and its counterpart SPS-treated at 900 °C for 15 min are shown in Fig. 4. In order to be taken as a reference, the representative plotted pattern of the calcined powder at 800 °C for 1 h was included in the same figure. In principle, both sintered specimens have a perovskite structure without the evidence of secondary phases. However, some studies suggest that both orthorhombic and tetragonal crystalline structures coexist at room temperature, which considerably enhances piezoelectricity due to the larger number of possible polarizable directions [23,26,27]. In this case, the tetragonal structure matched with the PLS-sintered sample and the SPS-sintered sample apparently developed an orthorhombic structure.

According to the corresponding phase diagram [20], for this composition, the system is close to a phase transition somewhere between the orthorhombic and tetragonal phases. Therefore, it is expected that the crystalline structure must be sensitive to thermodynamic variables such as pressure, temperature and composition. Thus, it is probable that different sintering processes might have induced the growth of different crystalline structures in the same powder. It is thought that these results can be attributed to the low alkaline elements loss during the process and to the axial pressure applied in the SPS process while the sample was sintered. It is worth mentioning that the latter has been studied in some materials [28–30] and it was observed that large enough mechanical stresses can induce phase transitions.

Regarding the dielectric properties, frequency dependent values of the real and imaginary parts of impedance constitute the total experimental data obtained. By using impedance plots and modeling those via equivalent circuits, it may allow the determination of frequency independent parameters related to the bulk properties, as it has been reported previously [31–33]. However, in our case, the experimental impedance data were only distributed on the high frequency region. Thus, as an alternative procedure, it was decided to use raw data in order to analyze the frequency dependent physical features. Fig. 5 shows the real part of the dielectric constant $\varepsilon'(\omega)$, plotted as a function of temperature. The magnitude of $\varepsilon'(\omega)$ given by $\varepsilon'(\omega) = gZ''/[\varepsilon_0\omega\{(Z')^2 + (Z'')^2\}]$, Z' and Z'' represent the real and imaginary parts of the impedance, respectively, while g is a geometrical factor, ω the angular frequency and $\varepsilon_0 = 8.854 \times 10^{-12}$ F/m.

At selected frequencies, the curves exhibit characteristic temperatures, indicated by the $\varepsilon'(\omega)$ peaks, which correspond to the expected orthorhombic–tetragonal and ferro-paraelectric transitions.

For the PLS sintered sample at 1120 °C, as shown in Fig. 5, there is no appreciable dispersion of $\varepsilon'(\omega)$ even when $T > T_C$ at 10 kHz and 100 kHz. This sample has T_{O-T} transition near room temperature, which confirms the XRD results. The inset shown in Fig. 5, was included in order to clarify this point. For this composition, $T_C \sim 354$ °C, this is comparable with data reported for samples synthesized through conventional ceramic processing [34–37]. The

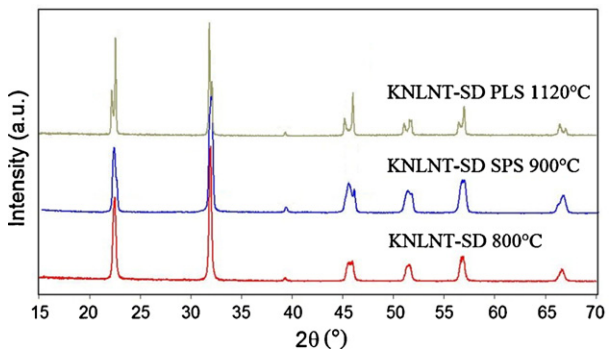

Fig. 4. X-ray diffraction patterns of KNLNT sintered samples, PLS-sintered at 1120 °C for 2 h, SPS-treated at 900 °C for 15 min and calcined powders at 800 °C for 1 h.

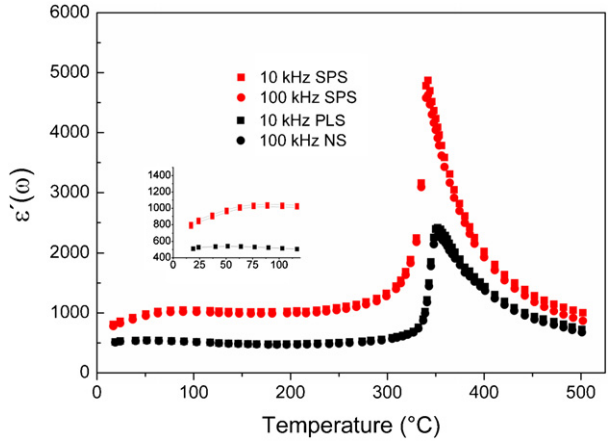

Fig. 5. Variation of dielectric constant with temperature for KNLNT, PLS-sintered at 1120 °C and SPS-treated 900 °C.

sample sintered at 900 °C by SPS has shown a trend similar to the sample sintered at 1120 °C, with considerably higher values of $\varepsilon'(\omega)$ at any temperature. As stated above, the possible existence of orthorhombic structure can be seen in Fig. 5, where a transition T_{O-T} may be assigned at around 80 °C, being highlighted in the inset in Fig. 5. Moreover, T_C has been shifted to a lower temperature (~442 °C). A possible explanation of the observed increment in the dielectric constant for the SPS sample could be attributed to the smaller grains [38], the higher density and the low deviation from ideal composition, explaining also both transitions, T_{O-T} and T_C.

The values obtained from the equation $\tan\delta = Z'(\omega)/Z''(\omega)$ are shown in Fig. 6 for both samples, PLS 1120 °C and SPS 900 °C. The dielectric losses in both samples are considerably low at room temperature and even near the Curie temperature (T_C). At room temperature (25 °C), the $\tan\delta$ (%) at 10 kHz and 100 kHz in both samples are 1.05, 1.24, and 2.37, 3.19, respectively. It was noticed that at low frequency, $\tan\delta$ increases rather quickly than at higher frequencies and increasing rapidly only when $T > T_C$ at 10 kHz. It is well known that the charge transport is the major contribution to the loss mechanisms. Thus, the $\tan\delta$ behaviour can be explained by the corresponding increment in the conductivity at higher temperatures.

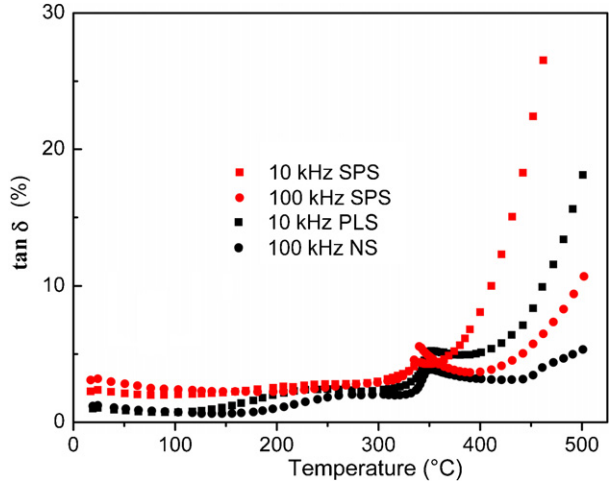

Fig. 6. Dielectric losses of KNLNT samples at 10 and 100 kHz, normal PLS-sintered 1120 °C and SPS-Sintered 900 °C.

Table 1
Coefficients and mechanical quality factors for KNLNT ceramics sintered by conventional PLS and SPS methods.

Coefficient	PLS 1120 °C	SPS 900 °C
ε_{33}^T	$464.5 - 3.0i$	$557.4 - 7.1i$
σ^p	$0.2360 - 3.9 \times 10^{-5}i$	$0.4215 - 4.9 \times 10^{-5}i$
$Q_m(c_{11}^p)$	90.62	261.5
s_{11}^E (10^{-12} m^2 N^{-1})	$11.80 - 0.13i$	$12.24 - 0.05i$
$Q_m(s_{11}^E)$	90.77	244.8
s_{12}^E (10^{-12} m^2 N^{-1})	$-2.786 + 0.031i$	$-5.158 + 0.020i$
d_{31} (10^{-12} C N^{-1})	$-55.86 + 0.28i$	$-66.15 + 0.58i$

The electrical admittance of a poled disk in the direction of its principal axis at the radial resonance is given by

$$Y = G + iB = i\left(\frac{2\pi^2 f a^2}{t}\right) \times \left(\varepsilon_{33}^T + 2d_{31}^2\left(\frac{c_{11}^p}{(1/(2 - \Im_1[2\pi f a\sqrt{(\rho/c_{11}^p)}])) - (1/(1+\sigma^p))}\right)\right) \quad (3.1)$$

Parameters like ρ (density), a (radius), t (thickness), and the oscillation frequency f are real numbers, but the rest of the variables are complex quantities, i.e. the piezoelectric constant d_{31}, the permittivity ε_{33}^T, Poissons' planar ratio, σ^p, and c_{11}^p. The last two properties are related to the standard compliance constants s_{11}^E and s_{12}^E. In addition, $\Im_1(z)$ is defined in terms of Bessel functions and the argument $z = 2\pi f a(\rho/c_{11}^p)^{1/2}$.

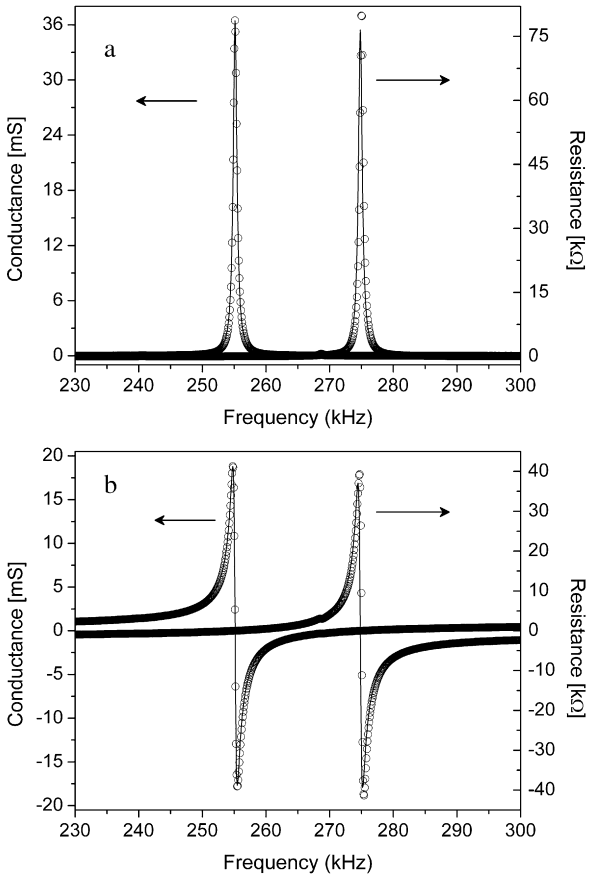

Fig. 7. Radial resonance and anti-resonance profiles of the KNLNT-SD PLS 1120 °C sample: (a) real parts and (b) imaginary parts.

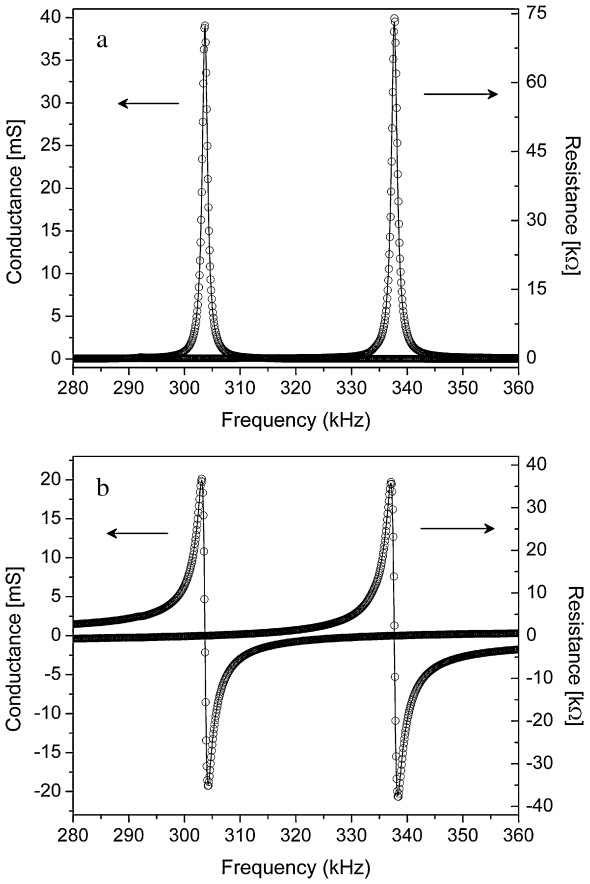

Fig. 8. Radial resonance and anti-resonance profiles of the KNLNT-SD SPS 900 °C sample: (a) real parts and (b) imaginary parts.

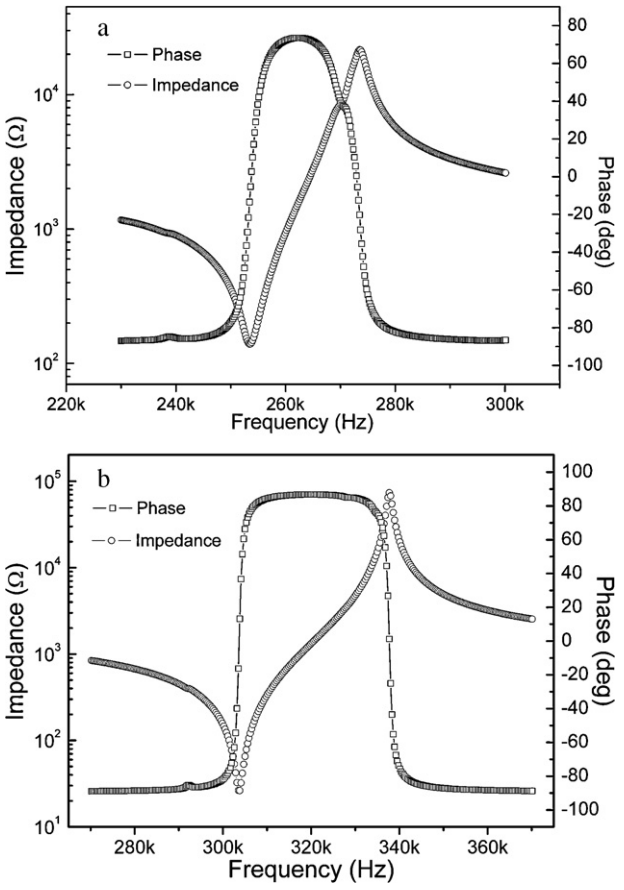

Fig. 9. Frequency dependence of impedance and phase for (a) KNLNT-SD PLS 1120 °C and (b) KNLNT-SD SPS 900 °C.

The aim of the aforementioned method [16,17] is to obtain the coefficients in Eq. (3.1) by solving, via an iterative numerical procedure, the set of nonlinear equations that result when complex experimental impedance or admittance are introduced into the piezoelectric resonance analytical solutions. Once the coefficients have been obtained, the resonance profiles are reconstructed by using Eq. (3.1) and compared with the experimental data. This comparison is a good test of the reliability of the obtained coefficients. For each parameter it is possible to define a quality factor, Q, as the absolute value of the ratio of the real to the imaginary component, although in this paper we are only reporting Q_m, i.e. the quality factor associated with the mechanical constants.

For comparison, k'_p was also calculated with the well known formula [39] that uses resonance and anti-resonance frequencies. This formula is generally used to find the value of the planar coupling factor. Nevertheless, as it is stated by our results, this expression overestimates its value.

In Fig. 7(a) and (b) the experimental results for the fundamental resonance and anti-resonant modes of the sample KNLNT-SD 1120 °C are shown, together with continuous curves for the real parts (Fig. 7(a)) of the admittance and the impedance, i.e. G and R, respectively; and the imaginary parts B and X (Fig. 7(b)). The continuous curves were calculated using Eq. (3.1) with the values of the constants determined by the iterative method that was mentioned earlier (Table 1).

Fig. 8(a) and (b) shows the curves of the same type as those depicted in Fig. 7, for the KNLNT-SD SPS 900 °C sample.

The imaginary contribution of piezoelectric parameters appearing in Eq. (3.1) is important in order to obtain good fitting between the experimental and the reconstructed resonance and anti-resonance profiles.

Fig. 9 shows the resonant (f_r) and anti-resonant (f_a) frequency maxima in the impedance measurement for KNLNT-SD PLS 1120 °C (a) and KNLNT-SD SPS (b). As it is clearly observed, the magnitude of $\Delta f\,(f_a - f_r)$ is larger for the SPS sintered sample than for the PLS specimen and considering the formula for k'_p calculation, the bigger the Δf, the higher the k'_p value. On the other hand, the change in the planar mode of the electromechanical coupling factor will be discussed further below.

Table 2 shows the values of k'_p, T_C, $\tan\delta$ and density for both samples. The sample sintered at 1120 °C has a k'_p of 0.41, while for the SPS sample is 0.50 with the iterative method considering losses, but when calculated by the resonance anti-resonance formula these values are 0.44 and 0.53. As it can be seen, the formula does not consider the different type of losses (i.e. the imaginary parts of the parameters) [16,17] and it can be assumed that the obtained values through this expression are overestimated. The increase of k'_p is remarkably improved by around 25% with respect to the normal sintered sample. It was observed that the orthorhombic phase exhibited higher values of k'_p, piezoelectric constant d'_{31}, permittivity ε^T_{33}, elastic compliances s^E_{11} and s^E_{12}, Poisson's ratio σ^p and the quality factor Q_m, than the tetragonal one. According to references [20,40,11], it is expected, for samples with similar composition,

Table 2
Piezoelectric properties for KNLNT ceramics.

Parameter	PLS 1120 °C	SPS 900 °C
k'_p (%)	41	50
T_C (°C)	352	342
$\tan\delta$ (%)	1.0 (10 kHz)	2.4 (10 kHz)
ρ (g/cm^3)	4.58	4.77

the outstanding performance of materials having tetragonal structure. The observed effect in this study can be attributed to the higher density obtained in the SPS sample. Saito and Takao [20] reported $k'_p = 0.505$ for similar composition but with higher Ta^{5+} content and with sintering conditions of 100% oxygen atmosphere. Li et al. [34] reported a k'_p of 0.40 for a similar composition using cold-isostatic pressing (CIP), while Rubio et al. [35] obtained a k'_p of 0.37 for the $(K_{0.38}Na_{0.52}Li_{0.04})(Nb_{0.86}Ta_{0.10}Sb_{0.04})O_{2.97}$ composition also with CIP. Zhao et al. [36] found 0.394 for the $[(Na_{0.535}K_{0.480})_{0.942}Li_{0.058}](Nb_{0.92}Ta_{0.08})O_3$ composition with normal sintering process. For d'_{31}, the values of −55.86 and −66.15 (pC/N) were obtained for PLS 1120 °C and SPS 900 °C, respectively. Rubio et al. [35] reported a value of −62.1 (pC/N) in their study, while Ringgaard and Wurlitzer found −45 (pC/N) for the $K_{0.5}Na_{0.5}NbO_3$ compound [37]. In addition, both samples have very high densities, 4.58 g/cm^3 for PLS 1120 °C and 4.77 g/cm^3 for SPS 900 °C. As it is well known, it is difficult to sinter alkali niobates with a stoichiometric composition due to the considerable alkaline cation losses. The composition variation produces the appearance of secondary phases with the decrease in piezoelectric properties. On the other hand, the optimum sintering temperature for KNN ceramics has a very narrow range for producing materials with small variation in their piezoelectric response [12].

4. Conclusions

The synthesis of KNLNT high quality powder was conducted in this study at relatively low temperature and short calcination time (800 °C for 1 h), with a particle size <0.2 μm. This result demonstrates that spray drying is a feasible method for the synthesis of KNN-doped ferroelectric ceramics. The synthesized powder was successfully sintered by conventional pressureless (PLS) sintering at 1120 °C for 2 h in air, leading to a sample of high density. However, the specimen sintered by the SPS technique at 900 °C for 15 min showed a higher density and better piezoelectric properties than the sample sintered by the conventional method. Notwithstanding the specimen sintered by SPS had an orthorhombic structure, it showed an enhancement in the piezoelectric properties. Thus, it can be assumed that this improvement is not only structural-related but sintering-dependant. It is important to underline the low sintering temperature used with the SPS method, which is 220 °C lower than the conventional PLS sintering, as well as the improvement in densification. Finally, the electromechanical coupling factor (k'_p), the piezoelectric parameter (d'_{31}), the mechanical quality factor Q_m, and the loss tangent ($\tan\delta$) of the sample sintered by SPS have shown an improvement as compared with those of the PLS sample.

Acknowledgements

The authors are indebted to SNI-CONACyT, México, ICyTDF (PIFUTP08-110), PAPIIT-UNAM (IN116610-3), as well as to the Nano-Materials and Nano-Technology Network of Instituto Politécnico Nacional for the access to SPS facilities. Special thanks to Omar Novelo Peralta for the SEM images acquisition. R. López-Juárez wants to acknowledge to Instituto de Investigaciones en Materiales -UNAM and CONACyT for doctoral fellowship.

References

[1] Y. Saito, H. Takao, T. Tani, T. Nonoyama, K. Takatori, T. Homma, T. Nagaya, M. Nakamura, Nature 432 (2004) 84–87.
[2] Q. Yin, S. Yuan, Q. Dong, C. Tian, J. Alloy Compd. 491 (2010) 340–343.
[3] F. Rubio-Marcos, J.J. Romero, M.G. Navarro-Rojero, J.F. Fernandez, J. Eur. Ceram. Soc. 29 (2009) 3045–3052.
[4] W. Yang, D. Jin, T. Wang, J. Cheng, Physica B 405 (2010) 1918–1921.
[5] D. Gao, K.W. Kwok, D. Lin, H.L.W. Chan, J. Mater. Sci. 44 (2009) 2466–2470.
[6] C.W. Ahn, C.S. Park, C.H. Choi, S. Nahm, M.J. Yoo, H.G. Lee, S. Priya, J. Am. Ceram. Soc. 92 (2009) 2033–2038.
[7] D. Gao, K.W. Kwok, D. Lin, H.L.W. Chan, J. Phys. D: Appl. Phys. 42 (2009) 035411.
[8] M. Jiang, X. Liu, G. Chen, C. Zhou, Mater. Lett. 63 (2009) 1262–1265.
[9] N.M. Hagh, K. Kerman, B. Jadidian, A. Safari, J. Eur. Ceram. Soc. 29 (2009) 2325–2332.
[10] A. Chowdhury, J. Bould, Y. Zhang, C. James, S.J. Milne, J. Nanopart. Res. 12 (2009) 209–215.
[11] T. Rojac, A. Benčan, H. Uršič, B. Malič, M. Kosec, J. Am. Ceram. Soc. 91 (2008) 3789–3791.
[12] Y. Wang, D. Damjanovic, N. Klein, E. Hollenstein, N. Setter, J. Am. Ceram. Soc. 90 (2007) 3485–3489.
[13] R. López, F. González, M.P. Cruz, M.E. Villafuerte-Castrejon, Mater. Res. Bull. 46 (2011) 70–74.
[14] M. Tokita, J. Soc. Powder Technol. Jpn. 30 (1993) 790–804.
[15] N. Tamari, T. Tanaka, K. Tanaka, I. Kondoh, M. Kawahara, M. Tokita, J. Ceram. Soc. Jpn. 103 (1998) 740–742.
[16] M. Algueró, C. Alemany, L. Pardo, A.M. González, J. Am. Ceram. Soc. 87 (2004) 209–215.
[17] M. Algueró, C. Alemany, L. Pardo, A.M. González, J. Phys. D: Appl. Phys. 28 (1995) 945–956.
[18] R. López, J. Zárate, E.A. Aguilar, J. Muñoz-Saldaña, J. Rare Earths 26 (2008) 670–673.
[19] F. Bezzi, A.L. Costa, D. Piazza, A. Ruffini, S. Albonetti, C. Galassi, J. Eur. Ceram. Soc. 25 (2005) 3323–3334.
[20] Y. Saito, H. Takao, Ferroelectrics 338 (2006) 17–32.
[21] Y. Chang, Z. Yang, L. Wei, J. Am. Ceram. Soc. 90 (2007) 1656–1658.
[22] Y. Guo, K. Kakimoto, H. Ohsato, Mater. Lett. 59 (2005) 241–244.
[23] P. Zhao, B. Zhang, R. Tu, T. Goto, J. Am. Ceram. Soc. 91 (2008) 3078–3081.
[24] E. Dowty, Am. Mineral. 61 (1976) 448–459.
[25] A. Millan, Cryst. Growth Des. 1 (2001) 245–254.
[26] H. Du, F. Tang, D. Liu, D. Zhu, W. Zhou, S. Qu, Mater. Sci. Eng. B 136 (2007) 165–169.
[27] Z. Yang, Y. Chang, B. Liu, L. Wei, Mater. Sci. Eng. A 432 (2006) 292–298.
[28] V.M. Timchenko, G.Y. Akimov, N.G. Labinskaya, Tech. Phys. 44 (1999) 156–160.
[29] P.E. Janolin, B. Dkhil, M. Davis, D. Damjanovic, N. Setter, Appl. Phys. Lett. 90 (2007) 152907.
[30] R.S. Chellappa, D. Chandra, S.A. Gramsch, R.J. Hemley, J.F. Lin, Y. Song, J. Phys. Chem. B 110 (2006) 11088–11097.
[31] J.R. McDonald, Impedance Spectroscopy: Emphasizing Solid Materials and Systems, Wiley, New York, 1987.
[32] A.K. Jonscher, Dielectric Relaxation in Solids, Chelsea Dielectric Press, London, 1983.
[33] J.T.S. Irvine, D.C. Sinclair, A.R. West, Adv. Mater. 2 (1990) 132–138.
[34] J. Li, Y. Zhen, B. Zhang, L. Zhang, K. Wang, Ceram. Int. 34 (2008) 783–786.
[35] F. Rubio-Marcos, P. Ochoa, J.F. Fernandez, J. Eur. Ceram. Soc. 27 (2007) 4125–4129.
[36] P. Zhao, R. Tu, T. Goto, B. Zhang, S. Yang, J. Am. Ceram. Soc. 91 (2008) 3440–3443.
[37] E. Ringgaard, T. Wurlitzer, J. Eur. Ceram. Soc. 25 (2005) 2701–2706.
[38] J. Li, K. Wang, B. Zhang, L. Zhang, J. Am. Ceram. Soc. 89 (2006) 706–709.
[39] Y. Chang, Z. Yang, L. Wei, B. Liu, Mater. Sci. Eng. A 437 (2006) 301–305.
[40] D. Lin, K.W. Kwok, H.L.W. Chan, J. Appl. Phys. 102 (2007) 034102.